Current-Injected Torque Ripple Reduction with Minimized Iron Loss in PMSMs

Litao Dai, *Member*, *IEEE*, Shuangxia Niu, *Senior Member*, *IEEE*, and Xin Yuan, *Member*, *IEEE*

***Abstract*—This letter presents a new current harmonic injection method to mitigate the inherent torque ripple in PMSMs. In contrast to conventional methods that aim to reduce torque ripple while minimizing copper loss, this study explores the optimal solution for minimized iron loss. The key of the proposed method involves injecting 6*n*-th *dq*-axis currents with carefully configured amplitude and phase, resulting in the generation of only (6*n*-1)-th winding current. This approach effectively avoids a significant increase in iron loss, which is the primary source of additional losses induced by the injected current. The effectiveness of the proposed method is validated through both finite element method and comparative experiments.**

***Index Terms*—Permanent magnet machine, loss, torque.**

I. Introduction

ACHIEVING smooth torque is crucial for precise and stable operation of permanent magnet synchronous machine (PMSM) drives [1]. However, PMSMs often suffer from torque ripples originate from three primary sources:

1. Spatial harmonics, which exist in the rotor and stator fluxes, as well as magnetic reluctance. The interaction of these harmonics results in cogging torque, synchronous torque ripple, and reluctance torque ripple [2].
2. Time harmonics, which are reflected in the current harmonics. Reducing current harmonics helps suppress torque ripple from this source. One approach is to design a current harmonic regulator within the control [3].
3. Mechanical issues, which may arise from manufacturing deviations and load misalignment [4].

Current injection is an efficient strategy for mitigating torque ripple [5]-[9]. This technique involves injecting current harmonics into the *d*- and *q*-axes to counteract inherent torque ripple. As research progresses, objectives have expanded from merely suppressing torque ripple to addressing the adverse effects induced by the injected harmonics. Particularly noteworthy is the emphasis on minimizing losses.

To achieve this goal, the optimal allocation of injected *d*-axis and *q*-axis harmonics is crucial. Theoretical solutions can be obtained by analyzing the parameters of *dq*-axes inductance and flux-linkage, as detailed in [5], [6], [7]. However, these parameters display nonlinearity across operating conditions. In this context, Ref. [8] investigates an analytical solution that considers the magnetic saturation effect. In contrast, an alternative method, independent of *dq*- parameters, involves offline collection of extensive motor data, constructing a surrogate model, and performing global optimization [9].

The focus of previous works [5]-[9] is to counteract inherent torque ripple through minimized current harmonic amplitudes, thereby reducing copper loss. However, these studies have overlooked the impact on iron loss. In practical situations, induced iron loss might surpass induced copper loss due to the iron loss being more susceptible to current harmonics.

Moreover, specific studies emphasize the importance of mitigating injected iron loss by integrating an iron-loss-related resistance into the equivalent *dq*-axis model and optimizing the *dq*-axes current. The main limitations of existing methods are as follows:

1. The conventional *dq*-axis model fails to differentiate between (6*n*-1)-th and (6*n*+1)-th winding current harmonics [10], treating them as the same 6*n*-th harmonic within the *dq*-axes. However, distinct iron loss characteristics are exhibited by different winding harmonics based on their frequencies.
2. Although certain studies have explored the utilization of multiple *dq*-axis circuits for analyzing winding harmonics [11], [12], the complexity of resolving multiple loss equations poses a challenge in achieving overall loss minimization.
3. The most critical challenge lies in accurately determining the equivalent parameters of the iron-loss resistances, given their variability during magnetic saturation conditions and with different current frequencies.

Additionally, certain studies reduce iron loss implementing optimal harmonic schemes derived from finite-element method (FEM) models into practical motor control [13], [14]. While theoretically robust, this approach necessitates thorough offline investigations and adjustments to the FEM-based iron loss using experimental data to achieve optimal reduction effects.

In summary, existing methods exhibit limitations in their effectiveness and simplicity in addressing torque ripple and additional iron loss.

To address the challenge of effectively suppressing injected iron loss, which often represents a significant portion of the total induced losses and can be difficult to reduce efficiently, this letter proposes an optimal harmonic injection method that strategically allocates *dq*-axis harmonics to induce only lower-order current harmonic in the windings, eliminating the need for introducing an iron-loss resistance or determining its parameters. This strategic allocation leads to a significant reduction in iron loss. Additionally, the method establishes a more simplified relation between *d*- and *q*-axis currents, rendering it easy to implement and suitable for both salient and non-salient PMSMs.

The letter is structured as follows: Section II explores the current injection effects. Section III develops the proposed method. Section IV presents the verification process, and Section V concludes the letter.

II. Analysis of Current Harmonic Injection

Fig. 1 provides an overview of the additional effects arising from harmonic current injection. The primary objective is to mitigate the inherent torque ripple originating from motor spatial harmonics, while the secondary outcome introduces additional copper and iron losses due to current harmonics.

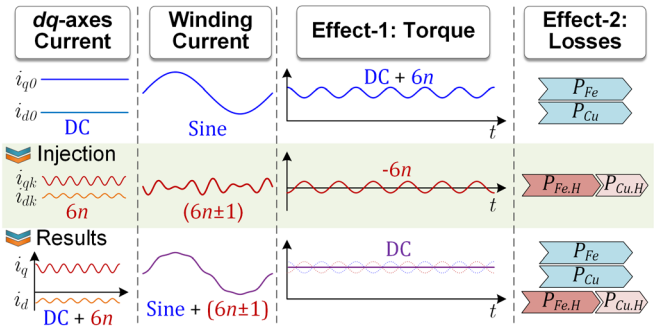

Fig. 1. Overview of additional effects of current harmonic injection.

A. Effect of Injected Current on Torque Ripple

For three-phase PMSMs, the spatial-harmonic-sourced torque ripple follows a general pattern of $6n$ orders [2]. In this case, the arbitrary order torque ripple can be expressed as:

$$T_{rp} = T_F \sin\left(k\theta_e + \varphi_{TK}\right) \tag{1}$$

where k, T_F, and φ_{TK} are the order, amplitude, and phase of torque ripple, and $k = 6,\ldots,6n$; θ_e is the electrical angle.

On the other hand, the time-harmonic-sourced torque, based on the dq-axis equivalent equation, is given by:

$$T_e = \frac{3}{2} p_N \left(\Lambda_0 + L_\Delta i_d\right) i_q \tag{2}$$

where p_N is the pole-pairs, Λ_0 is the PM flux-linkage, and L_Δ denotes the difference between d- and q- inductances, ($L_\Delta = L_d - L_q$). Notably, i_d and i_q represent the d- and q- axis currents, which can contain harmonics, as shown below:

$$\begin{cases} i_d = i_{d0} + i_{dk} = i_{d0} + I_{dk} \sin\left(k\theta_e + \varphi_{dk}\right) \\ i_q = i_{q0} + i_{qk} = i_{q0} + I_{qk} \sin\left(k\theta_e + \varphi_{qk}\right) \end{cases} \tag{3}$$

where i_{d0} and i_{q0} denote the dc components, while i_{dk} and i_{qk} represent the ac components in dq- axis. I_{dk}, I_{qk} and φ_{dk}, φ_{qk} indicate the amplitude and initial phase of the harmonics.

By substituting (3) into (2), the time-sourced torque ripple can be derived, its k -th fluctuation component is given by:

$$T_h = T_{HJ} \sin\left(k\theta_e + \varphi_{HJ}\right) \tag{4}$$

where: $T_{HJ} = \sqrt{A_1^2 + A_2^2 + 2A_1A_2\cos\left(\varphi_{qk} - \varphi_{dk}\right)}$,

$$\varphi_{HJ} = \varphi_{dk} + \arctan\left(\frac{A_1 \sin\left(\varphi_{qk} - \varphi_{dk}\right)}{A_1 \cos\left(\varphi_{qk} - \varphi_{dk}\right) + A_2}\right),$$

and $A_1 = 1.5 p_N \left(\Lambda_0 + L_\Delta i_{d0}\right) I_{qk}$, $A_2 = 1.5 p_N L_\Delta I_{dk} i_{q0}$.

It is observed that the time-sourced torque ripple shares the same frequency as the spatial-sourced torque ripple ($k = 6n$). Therefore, by adjusting the parameters $\{I_{dk}, \varphi_{dk}, I_{qk}, \varphi_{qk}\}$, it is possible to achieve mutual cancellation of these two types of torque ripple when the following conditions are met:

$$T_{HJ} = T_F, \quad \varphi_{HJ} = \varphi_{TK} + \pi \tag{5}$$

B. Effect of Injected Current on Losses

The $6n$-th dq-axis current can generate both $(6n\pm1)$-th winding current harmonics based on the following correlations:

$$\boldsymbol{i}^s_{abc} = \boldsymbol{P}^{-1}\left(\theta_e\right) \boldsymbol{i}^r_{dqs} \tag{6}$$

where $\boldsymbol{i}^s_{abc} = \begin{bmatrix} i_{1-k} & i_{2-k} & i_{3-k} \end{bmatrix}^T$ denotes the current harmonics in three-phase windings. Also, $\boldsymbol{i}^r_{dqs} = \begin{bmatrix} i_{dk} & i_{qk} \end{bmatrix}^T$, and $\boldsymbol{P}^{-1}\left(\theta_e\right)$ represents the inverse Park's transformation matrix.

Furthermore, the winding current harmonics contribute to the additional copper loss $P_{Cu.H}$ and iron loss $P_{Fe.H}$, given by:

$$\begin{aligned} P_{Fe.H} &= \sum_{k_i = 6n\pm1} \int \left[A_e \left(k_i f\right)^2 B^2_{c,k_i} + A_h \left(k_i f\right) B^2_{c,k_i} \right] dv \\ P_{Cu.H} &= \sum_{k_i = 6n\pm1} 3 I^2_{ph.k_i} R_{ph} \end{aligned} \tag{7}$$

where k_i is the order of winding current harmonic, $I_{ph.ki}$ is the rms value of the k_i-th current, R_{ph} is the winding resistance, A_e and A_h are the coefficients for eddy current and hysteresis losses, $B_{c,ki}$ is the iron flux density caused by the k_i-th current, v is the iron volume, and f is the electrical frequency.

It is worth noting that the copper loss is solely proportional to the amplitude of the winding harmonics. In contrast, the iron loss is influenced by both the amplitude and frequency of the winding harmonics, following a power law relationship of 1-2.

III. Methodology

An overall comparison of different current-injected torque ripple reduction methods is shown in Fig. 2.

A. Conventional Current Harmonic Injection Methods

Conventional current injection methods can be classified into analytical solution [5]-[8] and surrogate solution [9]. Analytical solutions aim to maximize torque ripple per harmonic ampere (MTRPHA) to obtain the solution of $\{I_{dk}, \varphi_{dk}, I_{qk}, \varphi_{qk}\}$.

On the other hand, surrogate model does not rely on dq-axis parameters. However, this method requires extensive data collection of input and output characteristics, followed by offline operations such as fitting and iterative optimization.

Importantly, both of these approaches solely focus on reducing copper loss as an additional objective, following the MTRPHA principle. They fail to consider the harmonic orders induced in the windings due to the injected dq-axis currents.

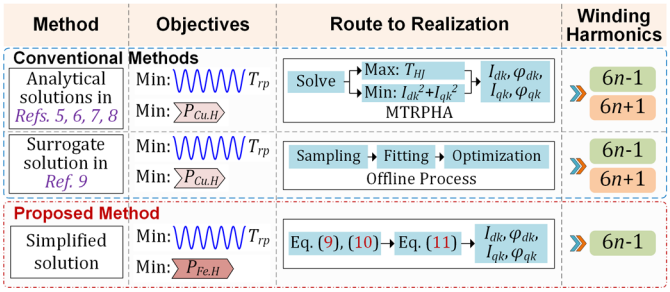

Fig. 2. Illustration of different current-injected methods.

B. Proposed Current Harmonic Injection Method

For an arbitrary k-th injection harmonic in dq-axis with the given $\{I_{dk}, \varphi_{dk}, I_{qk}, \varphi_{qk}\}$, through the transformation in (6), the winding harmonics $\begin{bmatrix} i_{1-k} & i_{2-k} & i_{3-k} \end{bmatrix}^T$ can be represented as:

$$i_{m-k} = i_{m,k+1} + i_{m,k-1}, \quad m = 1,2,3 \tag{8}$$

$$\begin{aligned} i_{m,k+1} &= \frac{1}{3}\left[I_{dk}\cos\varphi_{dk} - I_{qk}\sin\varphi_{qk}\right]\sin\left((k+1)\theta_e - (m-1)\frac{2\pi}{3}\right) + \\ &\quad \frac{1}{3}\left[I_{dk}\sin\varphi_{dk} + I_{qk}\cos\varphi_{qk}\right]\cos\left((k+1)\theta_e - (m-1)\frac{2\pi}{3}\right) \\ i_{m,k-1} &= \frac{1}{3}\left[I_{dk}\cos\varphi_{dk} + I_{qk}\sin\varphi_{qk}\right]\sin\left((k-1)\theta_e + (m-1)\frac{2\pi}{3}\right) + \\ &\quad \frac{1}{3}\left[I_{dk}\sin\varphi_{dk} - I_{qk}\cos\varphi_{qk}\right]\cos\left((k-1)\theta_e + (m-1)\frac{2\pi}{3}\right) \end{aligned}$$

A specialized solution for the above equation can completely eliminate high-frequency winding harmonics, as shown below:

$$I_{dk} = I_{qk} = I_{wk}, \quad \varphi_{dk} = \varphi_{qk} - \frac{\pi}{2} = \varphi_{wk} \tag{9}$$

By substituting (9) into (8), the three-phase winding currents can be expressed as:

$$i_{m-k} = \frac{2}{3} I_{wk}\sin\left((k-1)\theta_e + \varphi_{wk} + (m-1)\frac{2\pi}{3}\right), \quad m = 1,2,3 \tag{10}$$

It is evident that the $(6n+1)$-th current harmonic is eliminated. In order to visually understand the relationship between winding harmonics and the variation of injected dq-axis currents, Fig. 3 shows the correlation of the $(6n\pm1)$-th winding harmonics when $I_{dk} = I_{qk}$, and $\varphi_\Delta = \varphi_{qk} - \varphi_{dk}$ vary from 0 to 2π. It verifies that the current allocation scheme proposed in (9) produces only the $(6n-1)$-th winding harmonic.

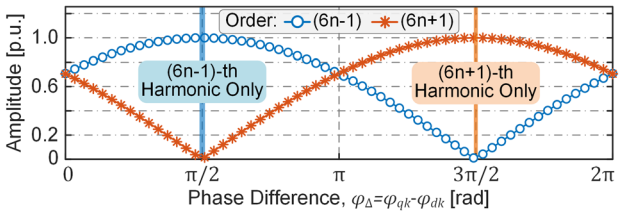

Fig. 3. Correlation between the amplitude of winding harmonics and the phase difference between d-axis and q-axis.

By combining (9) with (1), (4), and (5), the injected current can be analytical determined as shown below:

$$\begin{aligned} I_{wk} &= \frac{T_F}{1.5 p_N \sqrt{\left(\Lambda_0 + L_\Delta i_{d0}\right)^2 + \left(L_\Delta i_{q0}\right)^2}} \\ \varphi_{wk} &= \varphi_{TK} + \pi - \arctan\left(\frac{\Lambda_0 + L_\Delta i_{d0}}{L_\Delta i_{q0}}\right) \end{aligned} \tag{11}$$

Alternatively, another way to determine the current solution involves conducting a parametric scan of the injected current in FEM or experimental test, ensuring the satisfaction of Eq. (9).

Moreover, the motor control block diagram is shown in Fig. 4. Particularly, the quasi-proportional resonant (QPR) regulator is used in current control. The QPR regulator is characterized by effective control of current harmonics [15], [16]. In the design of QPR, achieving a high-bandwidth frequency current tracking and ensuring reliable response can be accomplished through fine-tuning the resonant coefficients [16] and phase compensation [17].

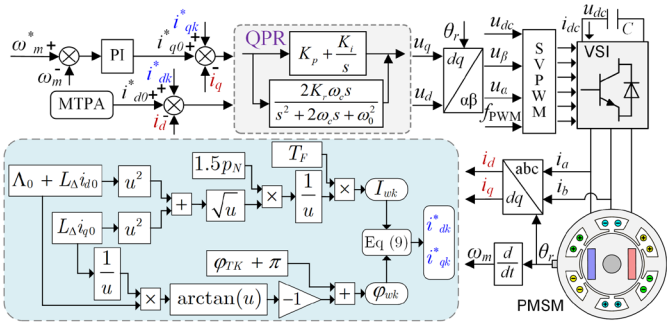

Fig. 4. Block diagram of the motor control system.

IV. Verification

This section provides a comprehensive verification for the proposed method in suppressing torque ripple and additional losses in comparison to advanced harmonic injection methods, namely Method-1 (M1) adopted in [4] that maintains $I_{dk} = 0$ and Method-2 (M2) proposed in [6], [7]. The verification process combines FEM and experimental investigations.

Initially, FEM is employed to compare torque ripple and losses among the aforementioned current excitation methods. TABLE I presents this comparison at a current density of 3.9 A/mm² and different rotational speeds. The comparison reveals significant reductions in torque ripple across the three methods, decreasing from 13.7% under sinusoidal current control to 1.62%, 1.81%, and 1.64%.

Furthermore, to clarify the differences in losses, the copper and iron losses resulting from injection are shown in Fig. 5. The iron loss is derived from FEM through the solution of the Bertotti model combined with high-precision transient field calculations. The three mitigation techniques exhibit varying impacts on injected losses. While operating under identical fundamental current conditions, there are increments in copper loss by 0.22 W, 0.2 W, and 0.26 W. Notably, distinct disparities emerge in iron loss, highlighting the proposed method with the lowest overall losses when the motor operates above 500 rpm.

TABLE I
TORQUE AND LOSSES COMPARISON BETWEEN DIFFERENT CURRENT EXCITATION METHODS THROUGH FEM INVESTIGATION

	Sine Current Excitation	Method-1	Method-2	Proposed Method
Torque Ripple, T_{rp}	13.7%	1.62%	1.81%	1.64%
P_{Cu} [W], @10.1 N·m	35.69	35.91	35.89	35.95
P_{Fe} [W], @200 rpm	5.57	5.66	5.65	5.60
P_{Fe} [W], @1000 rpm	31.87	32.61	32.55	32.31
P_{Fe} [W], @2000 rpm	73.90	76.10	75.76	75.51

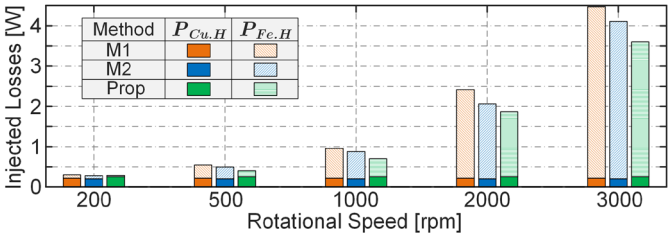

Fig. 5. Comparison of additional losses for different injection methods.

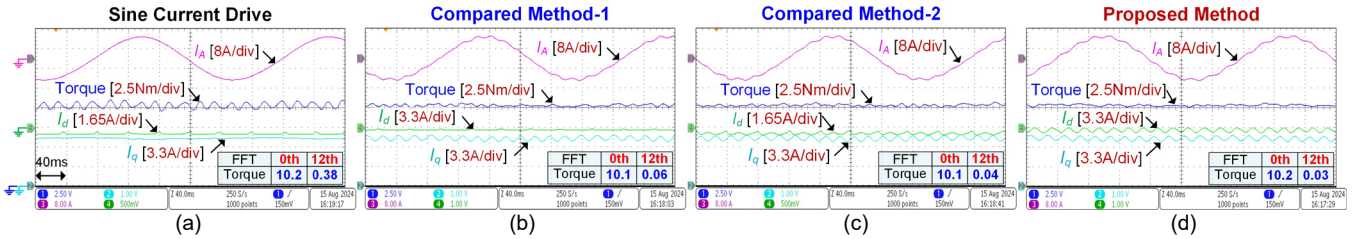

Fig. 7. Test waveforms under different current excitation methods. (a) Sine current. (b) Method-1 [4]. (c) Method-2 [6], [7]. (d) Proposed method.

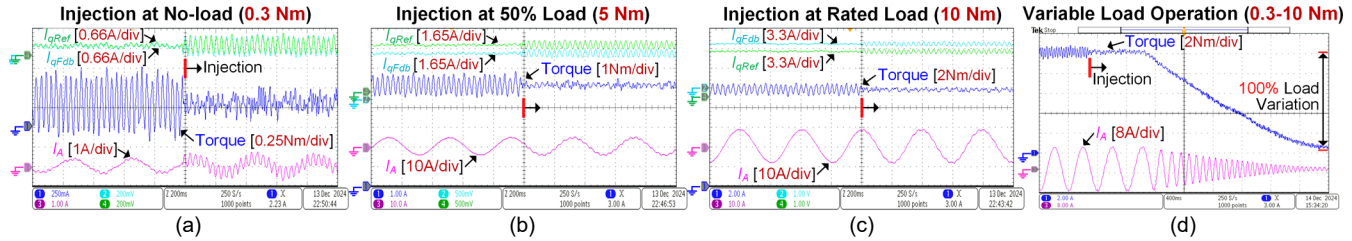

Fig. 9. Performance of varying load tests using the proposed method: (a) Harmonic injection switching at no-torque load. (b) Injection at 50% load. (c) Injection at rated load. (d) Operation under variable load conditions.

The test platform is shown in Fig. 6. The four current excitation methods are applied for motor control, and their corresponding test waveforms are presented in Fig. 7.

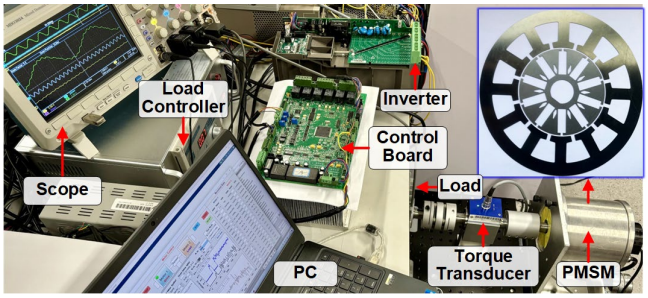

Fig. 6. Test platform and the investigated PMSM.

In Fig. 7 (a), sinusoidal current driving is applied, displaying stable i_d and i_q currents but noticeable 12th-order torque ripple. Fig. 7(b), (c), and (d) show different current injection methods for effectively suppressing torque ripple. Importantly, these methods exhibit distinct winding and dq-axis waveforms. Additionally, FFT analysis was performed on the four excitation currents, and the results are presented in Fig. 8.

While the winding current obtained from the proposed method shows increased total harmonic distortion (THD) due to larger single-sided current harmonics, it shows a notable reduction in higher-order current harmonics. This reduction can be advantageous in mitigating additional iron losses induced by high-frequency currents.

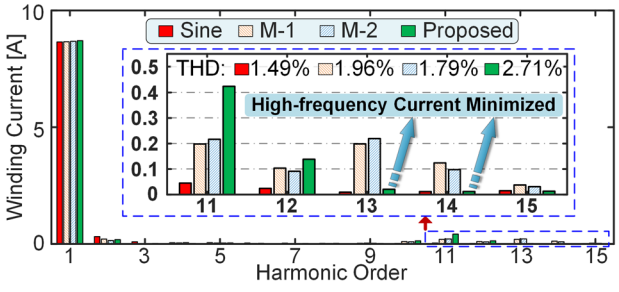

Fig. 8. FFT analysis of the test currents of different control methods.

To validate the effectiveness of the proposed torque ripple reduction method under varying load conditions, harmonic injection switching experiments were conducted across different load scenarios. The results are illustrated in Fig. 9, displaying phase current, shaft torque, as well as reference and actual i_q currents. The i_q current demonstrates good tracking capability. Furthermore, the comparative results highlight a significant reduction in torque ripple across a range of load conditions, affirming the smooth operation of the motor throughout the entire load spectrum, as shown in Fig. 9(d).

V. Conclusion

This letter introduces a novel current injection strategy for PMSMs, offering a specialized solution that efficiently reduces torque ripple and minimizes iron loss by optimizing the correlation between d- and q-axis currents.

Indeed, the proposed method, along with conventional Methods 1 and 2, all demonstrate effective torque ripple reduction. However, specific differences can be evaluated and summarized as follows:

1. **Loss Reduction**: The proposed method minimizes induced iron loss by using low-order current harmonics, making it well-suited for medium-to-high speeds, while Method-2 uses lower injected current amplitudes, more appropriate for low speeds.
2. **Usability**: Method-2 involves intricate dq-axis current relationships and relies on motor parameters, in contrast to the simple and direct dq- relationships in the proposed method and Method-1, enhancing user-friendliness.
3. **Computational Burden**: Method-1 imposes the lightest computational load, focusing primarily on controlling q-axis current harmonics.

References

[1] T. M. Jahns and W. L. Soong, "Pulsating torque minimization techniques for permanent magnet AC motor drives-a review," *IEEE Trans. Ind. Electron.*, vol. 43, no. 2, pp. 321-330, April 1996.

[2] L. Dai, S. Niu, W. Zhang, J. Gao and S. Huang, "Harmonic Modeling and Ripple Suppression of Electromagnetic Torque in IPMSMs," *IEEE Trans. Ind. Electron.*, vol. 71, no. 12, pp. 16223-16233, Dec. 2024.

[3] Z. Lyu, L. Wu, J. Yi and S. Yang, "Hybrid Frame-Based Current Control Scheme for LC-Equipped PMSM With Non-Sinusoidal Back-EMF," *IEEE Trans. Power Electron.*, vol. 38, no. 5, pp. 5994-6004, May 2023.
[4] S. -H. Park, J. -C. Park, S. -W. Hwang, J. -H. Kim, H. -J. Park and M. -S. Lim, "Suppression of Torque Ripple Caused by Misalignment of the Gearbox by Using Harmonic Current Injection Method," *IEEE/ASME Trans. Mech.*, vol. 25, no. 4, pp. 1990-1999, Aug. 2020.
[5] J. Qu, J. Jatskevich, C. Zhang and S. Zhang, "Torque Ripple Reduction Method for Permanent Magnet Synchronous Machine Drives With Novel Harmonic Current Control," *IEEE Trans. Energy Convers.*, vol. 36, no. 3, pp. 2502-2513, Sept. 2021.
[6] G. Feng, C. Lai and N. C. Kar, "An Analytical Solution to Optimal Stator Current Design for PMSM Torque Ripple Minimization With Minimal Machine Losses," *IEEE Trans. Ind. Electron.*, vol. 64, no. 10, pp. 7655-7665, Oct. 2017.
[7] G. Feng, C. Lai, and N. C. Kar, "Practical testing solutions to optimal stator harmonic current design for PMSM torque ripple minimization using speed harmonics," *IEEE Trans. Power Electron.*, vol. 33, no. 6, pp. 5181–5191, Jun. 2018.
[8] B. Zheng, J. Zou, Y. Xu, X. Lang and G. Yu, "Torque Ripple Suppression Based on Optimal Harmonic Current Injection in Dual Three-Phase PMSMs Under Magnetic Saturation," *IEEE Trans. Ind. Electron*, vol. 69, no. 6, pp. 5398-5408, June 2022.
[9] J. Qu, P. Zhang and J. Jatskevich, "Harmonic Current Optimization for Torque Ripple Reduction in Permanent Magnet Synchronous Machine Drives Based on Torque Ripple Surrogate Model," *IEEE Trans. Power Electron.*, vol. 39, no. 5, pp. 5108-5120, May 2024.
[10] J. Kim, S. -W. Ryu, M. S. Rafaq, H. H. Choi and J. -W. Jung, "Improved Torque Ripple Minimization Technique With Enhanced Efficiency for Surface- Mounted PMSM Drives," *IEEE Access*, vol. 8, pp. 115017-115027, 2020.
[11] J. Qu, P. Zhang, C. Zhang, and S. Zhang, "Torque ripple reduction method for interior permanent magnet synchronous machine drives with minimal loss, " *Proc. IEEE Energy Convers. Congr. Expo. (ECCE)*, Oct. 2022, pp. 1–7.
[12] H. Zhang, M. Dou, and J. Deng, "Loss-minimization strategy of nonsinusoidal back EMF PMSM in multiple synchronous reference frames," *IEEE Trans. Power Electron.*, vol. 35, no. 8, pp. 8335–8346, Aug. 2020.
[13] N. Nakao and K. Akatsu, "Torque ripple suppression of permanent magnet synchronous motors considering total loss reduction," *2013 IEEE Energy Conversion Congress and Exposition*, Denver, CO, USA, 2013, pp. 3880-3887.
[14] V. Varvolik et al., "Comparative Study on Torque Ripple Reduction Considering Minimum Losses for Synchronous Reluctance Motor Drives," *IEEE Trans. Transport. Electrific.*, vol. 10, no. 3, pp. 6527-6538, Sept. 2024.
[15] C. Du et al., "A Deadbeat Predictive Current Harmonics Suppression Method for IPMSM Based on Quasi Proportional Resonant Control," *IEEE Trans. Power Electron.*, vol. 39, no. 11, pp. 14909-14922, Nov. 2024.
[16] J. Xu, S. Guo, H. Guo and X. Tian, "Fault-Tolerant Current Control of Six-Phase Permanent Magnet Motor With Multifrequency Quasi-Proportional-Resonant Control and Feedforward Compensation for Aerospace Drives," *IEEE Trans. Power Electron.*, vol. 38, no. 1, pp. 283-293, Jan. 2023.
[17] A. G. Yepes, F. D. Freijedo, Ó. Lopez and J. Doval-Gandoy, "Analysis and Design of Resonant Current Controllers for Voltage-Source Converters by Means of Nyquist Diagrams and Sensitivity Function," *IEEE Trans. Ind. Electron.*, vol. 58, no. 11, pp. 5231-5250, Nov. 2011.